ACS Catalysis

Research Article

pubs.acs.org/acscatalysis

Synthesis of Monodisperse Plasmonic Au Core–Pt Shell Concave Nanocubes with Superior Catalytic and Electrocatalytic Activity

Haijuan Li,[†] Haoxi Wu,[†,‡] Yujuan Zhai,[†] Xiaolong Xu,[†] and Yongdong Jin*[,†]

[†]State Key Laboratory of Electroanalytical Chemistry, Changchun Institute of Applied Chemistry, Chinese Academy of Sciences, Changchun 130022, Jilin, China

[‡]University of the Chinese Academy of Sciences, Beijing 100039, China

Supporting Information

ABSTRACT: This work describes a facile and effective method for synthesis of concave Au@Pt nanocubes via a galvanic replacement process using preformed Au@Ag truncated nanocubes as templates. We found that the as-prepared concave Au@Pt nanocubes exhibit a unique plasmonic optical property and catalytic activity higher than that of a commercial Pt black catalyst in the catalytic reduction of *p*-nitrophenol into *p*-aminophenol by $NaBH_4$, and more importantly, the as-prepared concave Au@Pt nanocubes exhibit significantly higher electrocatalytic activity and greater durability for the ethanol oxidation reaction in alkaline media than commercial Pt black. The as-synthesized plasmonic Au core–Pt shell nanocubes, because of their well-defined concave core–shell nanostructure and high level of electrocatalytic performance, may find promising potential applications in various fields, such as ethanol fuel cells.

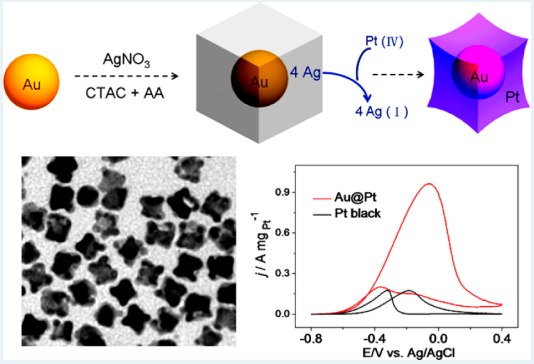

KEYWORDS: *platinum, concave, catalyst, gold, nanostructure*

Noble metal-based nanomaterials have been widely used as high-performance catalysts in fields ranging from chemical production and energy conversion and storage to environmental protection.[1−5] Among all of these nanomaterials, platinum (Pt)-based catalysts are very attractive because Pt is an indispensable component of many catalysts and electrocatalysts used in industrial processes and commercial devices because of its unique catalytic properties.[6] However, in view of the costliness of using Pt and the strong public demand, the fabrication of high-performance (activity, selectivity, and durability) Pt-based catalysts as inexpensively as possible is extremely urgent. To this end, intensive research has been recently focused on reducing the level of Pt loading and providing more active sites in the catalyst.[7−12] Until now, various Pt nanostructures, such as nanospheres, nanodendrites, nanofibers/nanowires, nanocages, nanotubes, nanosheets, and concave nanocubes, have been successfully synthesized.[13−20] Because of their unusual facets and negative curvature, nanocrystals with a concave structure have recently received attention for a number of applications related to catalysis, electrocatalysis, optical sensing, and electrochemiluminescence.[21−26]

Combining Pt with another metal (e.g., Pd,[27−31] Au,[7,32−39] Fe,[40] etc.) to generate bimetallic nanocrystals is an effective way to reduce the level of Pt loading and enhance the catalytic performance of a catalyst. It also has been demonstrated that bimetallic nanocatalysts often exhibit improved physical and chemical properties versus those of their monocomponent counterparts, as they provide more opportunities to optimize the catalytic performance by modulating the transfer of charge between different metals, local coordination environment, lattice strain, and surface element distribution.[1] So far, several types of important Pt-based bimetallic nanostructures (e.g., dendrites,[27−29,32] core–shells,[7,31,34−39] and two-dimensional nanomembranes[30]) have been successfully prepared.

Among various Pt-based bimetallic nanostructures, the core–shell nanostructure represents an elegant and highly interesting class of catalysts.[7,31,34−39] For instance, compared with monocomponent Pt nanoparticles (NPs), bimetallic Pd@Pt[31] and Au@Pt[34−39] core–shell NPs exhibit higher activities for the oxygen reduction reaction and enhanced CO tolerance for hydrogen activation, respectively.

Aiming to combine the fascinating properties of Au, such as its excellent chemical stability, its lower susceptibility to oxidation and corrosion in the catalytic reactions,[38] and its versatile nanoplasmonic properties (critical for integrated applications)[41−43] with high catalytic activity of nonspherical Pt nanostructures, we report herein for the first time a general and effective route for preparing monodisperse Au core–Pt shell concave nanocubes. The as-prepared bimetallic concave nanocubes exhibit not only unique plasmonic optical properties but also superior catalytic and electrocatalytic activities

Received: March 25, 2013
Revised: July 24, 2013
Published: July 26, 2013

   dx.doi.org/10.1021/cs400223g | ACS Catal. 2013, 3, 2045−2051

compared to those of commercial Pt black. As a model reaction, we choose the reduction of *p*-nitrophenol by $NaBH_4$ to *p*-aminophenol to evaluate the (plasmonic) catalytic activity of the as-prepared Au@Pt concave nanocubes; it has already been demonstrated that the reduction reaction can be catalyzed by noble metal NPs.[3,44,45] The Au@Pt concave nanocubes exhibit far better catalytic activity than commercial Pt black catalysts. More importantly, our concave Au@Pt nanocubes exhibit significantly higher electrocatalytic activity for the ethanol oxidation reaction (EOR) than commercial catalysts.

EXPERIMENTAL SECTION

Chemicals. Gold(III) chloride tetrahydrate ($HAuCl_4 \cdot 4H_2O$, ≥99.0%), potassium platinum(IV) chloride (K_2PtCl_6, ≥99.0%), and L-ascorbic acid (AA, ≥99%) were obtained from Sinopharm Chemical Reagent Co., Ltd. Silver nitrate ($AgNO_3$, ≥99%), sodium borohydride ($NaBH_4$, 99%), polyvinylpyrrolidone (PVP, MW of ~55000), cetyltrimethylammonium bromide (CTAB, ≥99%), cetyltrimethylammonium chloride (CTAC, 25 wt % in H_2O), and a Nafion 117 solution (5% in a mixture of lower aliphatic alcohols and water) were all obtained from Sigma-Aldrich and used as received. In all experiments, we used deionized water with a resistivity of 18 MΩ, which was prepared using an ultrapure water system (Millipore).

Synthesis of Au NPs. The monodisperse Au NPs were prepared by two steps according to the literature.[46] First, we made small Au NPs (~3 nm in diameter). A 42.5 μL aliquot of a 1% $HAuCl_4$ solution was added to 5 mL of a 100 mM CTAB solution at 27 °C. After this combination had been gently mixed, 0.3 mL of a 10 mM ice-cold $NaBH_4$ solution was added all at once, followed by rapid inversion mixing for 2 min. The 3 nm Au NP solution was kept undisturbed for 3 h at 27 °C to ensure complete decomposition of the $NaBH_4$ remaining in the solution. Then a total volume of 0.6 mL of the 3 nm Au NPs was added to a mixture of 12 mL of a $HAuCl_4$ solution (0.5 mM), 12 mL of a CTAC solution (200 mM), and 9 mL of an AA solution (100 mM). The final mixture turned from colorless to red within 1 min, indicating the formation of larger Au NPs. After 1 h, the products were collected by centrifugation (15000 rpm for 20 min) and then washed with water once; the final product was diluted to 2 mL with water.

Synthesis of Au@Ag Truncated Nanocubes. In a typical procedure, 1 mL of the Au NPs seeds and 9 mL of a CTAC (20 mM) aqueous solution were mixed in a 25 mL vial. After the mixture had been heated at 60 °C for 20 min while being magnetically stirred, 1 mL of an aqueous $AgNO_3$ solution (2 mM) and an aqueous solution of AA (50 mM) and CTAC (40 mM) were simultaneously injected at a rate of 0.2 mL/min using a flow injection analysis system. The volume of AA (50 mM) added to the reaction solution was kept the same as that of $AgNO_3$. After injection, the concentration of $AgNO_3$ in the final solutions was 0.17 mM. During the injection, the reaction mixture turned from red to brownish-yellow. After 4 h, the vials were cooled in an ice bath. The products were collected by centrifugation (15000 rpm for 15 min) and then washed with water once, and the final product was diluted to 2 mL.

Synthesis of Concave Au@Pt NPs. The concave Au@Pt nanocube was prepared via a galvanic replacement reaction between the Au@Ag truncated nanocubes and aqueous K_2PtCl_6 solution. In a typical procedure, 0.8 mL of the Au@Ag was redispersed in an 8 mL solution of PVP (0.5 wt %) and CTAB (0.1 M). Then, the Au@Ag truncated nanocubes were heated at 100 °C for 2 min followed by seven additions of 20 μL of a 0.1% K_2PtCl_6 solution. The color of the mixture changed to dark bluish. The final product was mixed with the same volume of 6 M HNO_3 to remove the AgCl precipitates and the unreacted silver. After that, the products were collected by centrifugation (10000 rpm for 10 min) and then washed with water twice.

Instrumentation and Measurements. Transmission electron microscopy (TEM) was conducted by using a FEI TECNAI F20 electron microscope with an accelerating voltage of 200 kV equipped with an energy-dispersive spectrometer. TEM samples were prepared by placing a drop of the final product on a carbon-coated copper grid and drying under ambient conditions. Both the UV−vis extinction spectra and the curves of extinction versus time were obtained using a Lambda 750 spectrometer (Perkin-Elmer, Wellesley, MA). All electrochemical tests were performed in a three-electrode cell connected to a CHI 832 electrochemical analyzer (CH Instruments, Chenhua Co., Shanghai, China). A Pt wire was used as the counter electrode, and Ag/AgCl in KCl (3 M) was used as a reference electrode. The working electrodes were fabricated on a glassy carbon electrode with an area of 0.07 cm^2. Before the catalyst had been loaded, the glassy carbon was polished with 1, 0.3, and 0.05 μm Al_2O_3 paste to ensure a mirrorlike surface. It was then cleaned in an ultrasonic bath. The suspension of Au@Pt or Pt black was dropped on the GC electrode. A thin layer of Nafion was placed on the nanocrystal-modified GC electrode by dropping 5 μL of an aqueous solution of Nafion (0.05%) to prevent erosion of the nanocatalysts during electrochemical measurements. The electrochemical active surface area (ECSA) was obtained by measuring the charges associated with the hydrogen desorption signals (Q_H) on the CV curves in 0.1 M $HClO_4$ in the hydrogen UPD region, assuming 210 $\mu C/cm^2$ for calibrating the desorption charge of a hydrogen monolayer on a Pt surface based on the following equation:

$$\mathrm{ECSA} = Q_H/(210m)$$

where Q_H is the charge for H_{upd} adsorption (determined by using $Q_H = 0.5Q$, where Q is the charge in the H_{upd} adsorption/desorption area obtained after double-layer correction) and m is the amount of Pt loaded (determined by inductively coupled plasma-atomic emission spectroscopy).[28]

RESULTS AND DISCUSSION

As depicted in Figure 1, the success of this synthesis relies on two steps: the synthesis of Au core−Ag shell (Au@Ag) truncated nanocubes[46] and the galvanic replacement between Ag of Au@Ag truncated nanocubes and $PtCl_6^{2-}$ ions. The synthesis of Au@Ag truncated nanocubes was conducted according to the previously reported method.[46] For the second

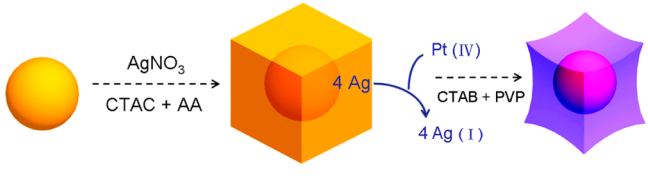

Figure 1. Schematic illustration of the two-step synthesis of the concave Au@Pt bimetallic nanocubes. Abbreviations: CTAC, cetyltrimethylammonium chloride; AA, L-ascorbic acid; CTAB, cetyltrimethylammonium bromide; PVP, polyvinylpyrrolidone.

dx.doi.org/10.1021/cs400223g | ACS Catal. 2013, 3, 2045−2051

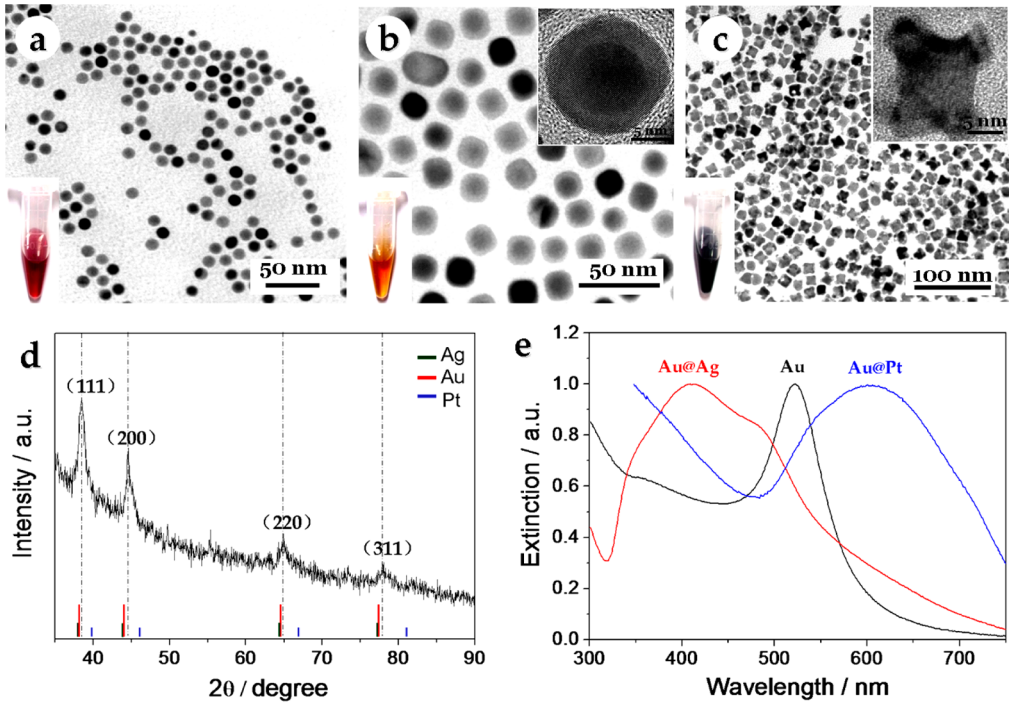

Figure 2. TEM images and photographs (inset) of Au NPs (a), Au@Ag truncated nanocubes (b), and concave Au@Pt nanocubes (c). (d) XRD pattern of the as-prepared concave Au@Pt nanocubes. (e) Typical UV−vis spectra of Au NPs, Au@Ag nanocubes, and concave Au@Pt nanocubes in aqueous solutions.

step, the transformation can be easily achieved via a galvanic replacement process (as described in eq 1) because the reduction potential of Ag is lower than that of Pt.[47,48] As the galvanic reaction proceeded, the Au@Ag truncated nanocubes disappeared gradually, accompanied by the formation of Au@Pt concave nanocubes with intact Au core and nanoporous shells of Pt.

$$4Ag + PtCl_6^{2-} \rightarrow Pt + 4AgCl + 2Cl^- \quad (1)$$

Figure 2a shows a TEM image of the Au core NPs used. The spherical Au NPs were nearly monodisperse, with an average size of 9.34 ± 0.9 nm (Figure S1 of the Supporting Information). The Au@Ag truncated nanocubes were first formed by depositing Ag on Au seeds. In a typical synthesis, with $AgNO_3$ as the precursor to elemental Ag, L-ascorbic acid (AA) as the reducing agent, and cetyltrimethylammonium chloride (CTAC) as the capping agent, monodisperse cubic Au@Ag core−shell NPs were formed because of the conformal overgrowth of Ag on the Au seeds. Figure 2b shows a typical TEM image of the Au@Ag truncated nanocubes obtained by injecting 1 mL volumes of $AgNO_3$ (2 mM) into aqueous suspensions containing 1 mL of Au seeds. The edge length of the resultant Au@Ag was ∼14.8 ± 1.6 nm (Figure S2 of the Supporting Information). The size of the resultant Au@Ag core−shell nanocrystals can be controlled by varying either the amount of $AgNO_3$ or the amount of Au seeds added to the reaction solution.[46] A clear difference in contrast can be observed between the Au core and the Ag shell because of the difference in atomic number and thus attenuation of electrons. It was clearly seen that essentially every cubic NP contained one Au NP seed in its center with a complete and smooth Ag coating (Figure S4 of the Supporting Information). It has been known that the choice of a capping agent can greatly influence the final shape of the nanocrystals as well as their sizes (e.g., Mirkin et al. have discovered that a simple change of the halide counterion from Br^- to Cl^- in the capping agent induces a dramatic change in the product morphology and yields a concave rather than convex cubic structure[21]). Xia et al.[46] have extensively examined the growth mechanism of Au@Ag nanocubes by investigating the effects of the capping agent [CTAC or cetyltrimethylammonium bromide (CTAB)] on the size and shape of the resultant core−shell nanocrystals. Their results indicated that because the oxidative etching power of CTAB is weaker than that of CTAC, CTAC worked much better than CTAB as a capping agent in the syntheses of both Au seeds and Au@Ag core−shell nanocubes.[46] CTAB was not ideal for the growth step because of the formation of water-insoluble AgBr upon the addition of an $AgNO_3$ solution, which was harder to be reduced than Ag^+ ions when AA was used as a reductant.

The Au@Pt concave nanocubes were then prepared by the galvanic replacement reaction between the Ag shells and aqueous K_2PtCl_6. As 4 mol of Ag can replace only 1 mol of K_2PtCl_6, the precursor Au@Ag truncated nanocubes became a concave nanostructure after the galvanic replacement reaction. Figure 2c shows a representative TEM image of the as-prepared concave Au@Pt nanocubes with an inhomogeneous shell. The apex−apex length of the concave Au@Pt nanocubes is 12.81 ± 2.05 nm (Figure S3 of the Supporting Information). In the previous methods,[49−51] the Pt shell thicknesses could be controlled by changing the solution composition. In this report, the Pt shell thicknesses can be controlled by changing the thickness of the Ag shell, which can be controlled by varying either the amount of $AgNO_3$ or the amount of Au seeds added to the reaction solution in the first step.[46] As shown in Figure S5 of the Supporting Information, some residual Ag still existed in the Au@Pt concave nanocubes. On the basis of inductively coupled plasma-atomic emission spectroscopy (ICP-AES), the

dx.doi.org/10.1021/cs400223g | ACS Catal. 2013, 3, 2045−2051

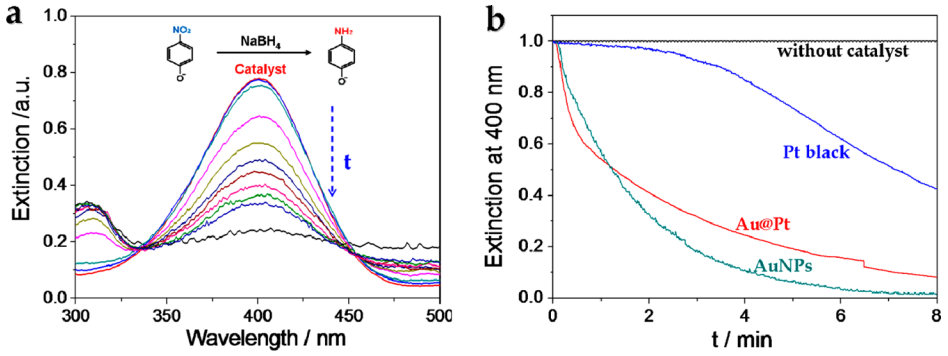

Figure 3. (a) UV−vis spectra of the catalytic system taken at different reaction times, indicating the decrease in the intensity for the peak at 400 nm associated with *p*-nitrophenol as the reduction of the NO_2 group to an NH_2 group. (b) Extinction (normalized to the initial point) at the peak position for *p*-nitrophenol (400 nm) as a function of time with the concave Au@Pt nanocubes and Pt black used as catalysts. All measurements were performed at room temperature (17 °C). In all experiments, the masses of the catalysts are kept constant (~18 μg/mL) and the concentrations of *p*-nitrophenol and $NaBH_4$ were 1.05×10^{-4} and 3.2×10^{-2} M, respectively.

Au/Ag/Pt mass ratio was measured to be ~69/8/23. The X-ray diffraction pattern recorded on the concave Au@Pt nanocubes (Figure 2d) shows the (111), (200), (220), and (311) reflections of the fcc structure of the metal, indicating the crystalline nature of the prepared concave nanocubes, which was consistent with the selected-area electron diffraction (SAED) pattern (Figure S6 of the Supporting Information). The Au@Pt particles do not show strong Pt diffraction reflections, indicating that the Pt shell is very thin. Because the surface plasmon (SP) band of plasmonic nanostructures is sensitive to various factors, including particle size, shape, and interparticle interactions,[4] we characterized the optical properties of the resulting concave Au@Pt nanocubes. Figure 2e shows UV−vis extinction spectra of Au NP seeds, Au@Ag truncated nanocubes, and concave Au@Pt nanocubes. The UV−vis extinction spectrum of the spherical Au NPs shows a peak at 520 nm, while the spectrum of the Au@Ag truncated nanocubes shows two characteristic peaks located at ca. 490 and 410 nm, representative of the Au core and the Ag shell, respectively. After the Ag/Pt replacement reaction, the SP band of the resulting Au@Pt concave nanocubes red-shifts to 610 nm, different from that of their monocomponent counterparts, indicating the Pt shell effect on Au NP's LSPR.[52]

The catalytic activities of the concave Au@Pt nanocubes in comparison with those of the commercial catalyst (Pt black) were first evaluated by employing the reduction of *p*-nitrophenol to *p*-aminophenol by $NaBH_4$ as a model system. In the reaction system, $NaBH_4$ greatly in excess as compared to *p*-nitrophenol was added so that the reduction rate could be thought to be independent of the concentration of $NaBH_4$, and the kinetic process of the reaction can be easily studied by simply monitoring the change of the intensity of the absorption peak at 400 nm correlated with *p*-nitrophenol versus time. As seen in Figure 3a, the magnitude of the absorption peak at 400 nm, after the addition of Pt-based catalysts, gradually decreased as the reduction reaction proceeded, indicating the reduction of the NO_2 group of *p*-nitrophenol to an NH_2 group.[3] No reaction occurred in the case of a catalyst-free mixture. Figure 3b shows that the as-prepared concave Au@Pt nanocubes exhibit catalytic activity higher than that of commercial Pt black. As compared with PtNPs (commercial Pt black), plasmonic Au NPs (Figure 2a) show superior catalytic activity in the reaction system (Figure 3b), indicating that the Pt shells of the as-prepared concave Au@Pt nanocubes are porous. This has been proven by electrochemical characterization. Figure 4 shows the

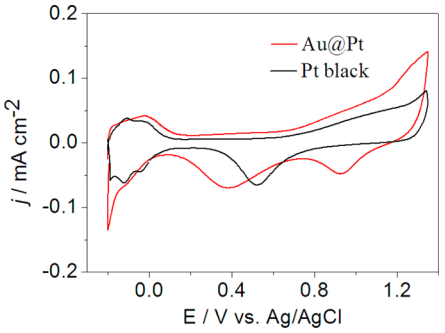

Figure 4. CVs (10th cycle) of the Au@Pt nanocubes and commercial Pt black electrodes in a 0.1 M $HClO_4$ solution at a scan rate of 50 mV/s.

representative cyclic voltammograms (CVs) obtained at 50 mV/s from −0.2 to 1.35 V versus Ag/AgCl for Au@Pt concave nanocubes and Pt black in 0.1 M perchloric acid. The CVs show typical potential regions for hydrogen adsorption and desorption between −0.2 and 0.15 V, the reduction of surfaces Pt−OH_{ad} between 0.3 and 0.7 V, and a pronounced feature corresponding to the gold oxide reduction peak at ~0.9 V in the negative scan direction, indicating that some gold sites remain exposed after the deposition of ultrathin Pt layers. As shown in Figure S7 of the Supporting Information, the obvious electrooxidation−reduction features of Ag around 0.3 V and the disappearance of the gold oxide reduction peak at ~0.9 V for a control Au@Ag electrode indicate that all of the Au NPs have been covered by Ag shells; therefore, there are no bare Au particles in final concave Au@Pt nanocubes.

By using hydrogen adsorption−desorption methods in conjunction with CVs, the electrochemical active surface area (ECSA) values for the Pt-based electrocatalysts were measured. The ECSA values for the concave Au@Pt nanocube and Pt black are 68.17 and 38.20 m^2/g, respectively. This indicates that the Au@Pt electrode had higher ECSA values, which would probably enhance the active sites in the electrochemical reactions. The electrocatalytic performance of the as-prepared concave Au@Pt nanocubes was further examined by choosing ethanol as a model molecule and compared with that of a commercial Pt black.[53−55] For EOR, the electrode reaction kinetics in an alkaline medium are higher than in an acidic medium,[53,55] so EOR experiments were conducted in alkaline medium. Panels a and b of Figure 5 [(a) mass activity, current

dx.doi.org/10.1021/cs400223g | ACS Catal. 2013, 3, 2045−2051

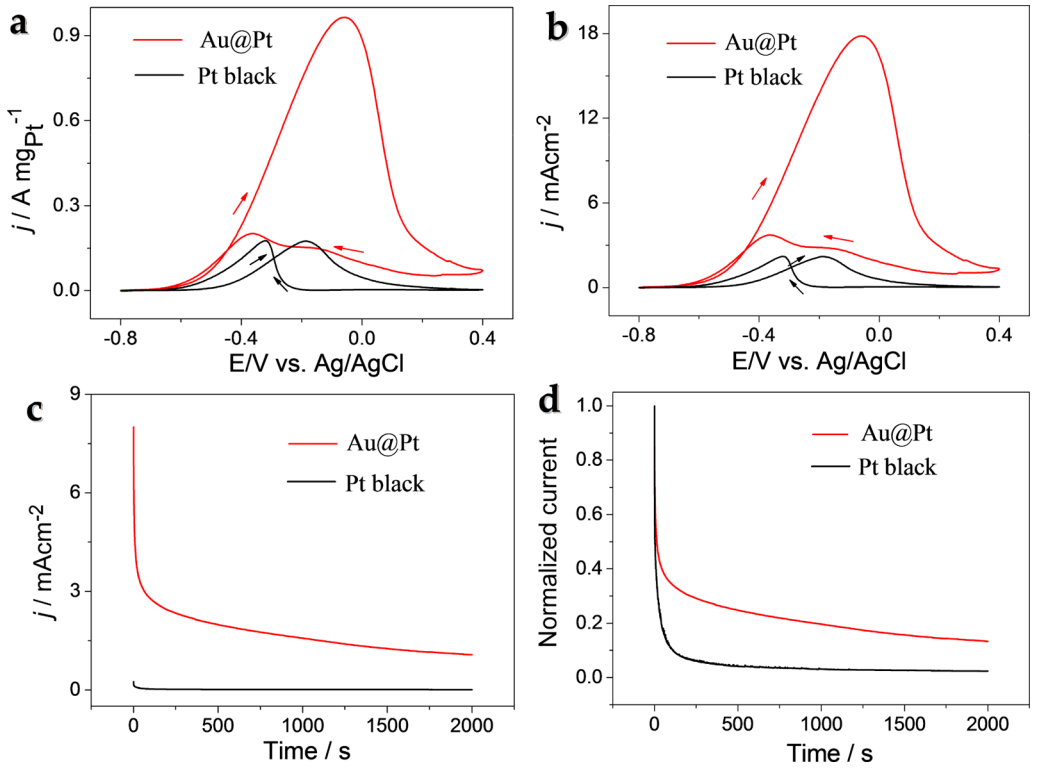

Figure 5. CVs [10th cycle; (a) mass activity and (b) specific activity] of Au@Pt (red line) and Pt black in a 1 M NaOH and 1 M ethanol solution at a scan rate of 50 mV/s. (c) Current density−time curves. (d) Normalized current density−time curves of the EOR catalyzed by the as-prepared concave Au@Pt nanocubes in a 1 M NaOH and 1 M ethanol solution at −0.06 V.

densities normalized to Pt mass; (b) specific activity, current densities normalized to ECSA] show the CVs of ethanol oxidation in a 1.0 M NaOH and 1.0 M C_2H_5OH solution at a scan rate of 50 mV/s on the Au@Pt (Pt loading of 17.7 μg/cm^2) and Pt black (Pt loading of 26.8 μg/cm^2) electrodes. The metal contents were evaluated by ICP-AES analysis. The onset potential for the ethanol oxidation on the Au@Pt electrode is ca. −0.5 V, which is 100 mV more negative than the value of ca. −0.4 V observed on Pt black electrocatalysts. The reduction of the onset anodic potential shows the significant enhancement of the kinetics of the ethanol oxidation reaction.[54] The magnitude of the anodic peak current density (j) in the forward scan is directly proportional to the amount of ethanol oxidized at the catalyst electrodes. The mass and specific activities of the Au@Pt electrode are ∼5.3 and ∼8.4 times higher, respectively, than those of the Pt black electrode. The ratio of peak currents on the forward and backward scans (i.e., I_f/I_b) could be used as a criterion to evaluate the poisoning of the catalyst surface by carbon-containing species (identified mainly as acyl) during EOR.[54−57] This ratio for the concave Au@Pt electrode (I_f/I_b = 4.85) was ∼4.8-fold higher than that for the commercial Pt black electrode (1.01), indicating a superior antipoison property of the concave Au@Pt nanocubes during the electrooxidation of ethanol. The electrochemical stability of the concave Au@Pt nanocubes and Pt black electrodes for ethanol electrooxidation was investigated by chronoamperometric experiments at a given potential of −0.06 V in a 1.0 M NaOH and 1.0 M C_2H_5OH solution (Figure 5c,d). The polarization current for the ethanol electrooxidation reaction shows a rapid decay in the initial period for both the samples, probably because of the formation of the intermediate species during the ethanol electrooxidation reaction in alkaline media. Nevertheless, the as-prepared Au@Pt catalyst has a much higher anodic current, and the current decay for the reaction on the Au@Pt electrode is significantly slower than that on the Pt black electrocatalysts. At the end of the 2000 s test, the oxidation current on the Au@Pt electrode is still ∼1.7 times higher than that on the Pt black electrode. These results showed that the as-prepared concave Au@Pt nanocube has long-term high catalytic activity for the ethanol electrooxidation reaction in alkaline media.

To investigate the effect of Au element on the catalytic activity of concave Au@Pt nanocubes for the EOR, we compared CVs of ethanol oxidation on the Au NP electrode with those on concave Au@Pt NPs and Pt black electrodes (see Figure S8a of the Supporting Information). The catalytic activity of EOR on Au NP electrodes is obviously far lower than those on Pt black and concave Au@Pt nanocube electrodes. The onset potentials for the concave Au@Pt and Pt black electrodes are 170 and 70 mV more positive, respectively, than that on the Au NP electrode, and the magnitudes of the specific activities of the concave Au@Pt NPs and Pt black electrodes are 13.3 and 1.7 times greater than that for Au NP electrodes, respectively. These data indicate that the reaction rate of EOR on Au NPs is smaller than that on platinum, as the EOR on platinum is easier than on gold.[58] Therefore, the EOR will start on platinum, which acts as primary active sites. In previous reports,[59,60] researchers have confirmed that the Au substrate can upshift the d-band energy of the Pt layer; a higher-lying d-band energy characterizes a more reactive surface that tends to bind adsorbates more strongly and enhances the kinetics of the dissociation reaction producing these adsorbates.

As shown in Figure S8b of the Supporting Information, during the EOR, the stability of the Au NPs is better than that

dx.doi.org/10.1021/cs400223g | ACS Catal. 2013, 3, 2045−2051

of Pt black. During the electrocatalytic ethanol oxidation in alkaline media, CO_{ads} can be produced by carbon−carbon bond breaking. The intermediate species CO_{ads} strongly adsorbs on the active sites of catalysts and hinders the reaction, while Au is a good catalyst for CO oxidation.[32] The previous study shows that Au enhances the activity and poisoning tolerance of Pt for alcohol oxidation as a result of an ensemble effect.[33,39,49−51] Therefore, it is tentatively deduced that the synergistic effect between Au and Pt contributes greatly to the high-level performance of the catalytic activity of concave Au@Pt nanocubes. It is likely that Pt acts as primary active sites for the degradation and dehydrogenation of alcohol, and the Au substrate improves the catalytic activity by upshifting the d-band energy of the Pt layer and extending the long-term stability of Au@Pt as Au can oxidize CO-like intermediate species to produce CO_2, releasing the active sites.[61]

The enhanced catalytic activity of the concave Au@Pt nanocube most likely originates from the synergistic effect between Au and Pt as well as that of the concave structure. Bimetallic nanocatalysts often show improved physical and chemical properties versus those of their monocomponent counterparts.[27−29,59−61] Surface areas and atomic surface structures play key roles in enhancing Pt catalytic activity.[21−23,62] The presence of concave structure provided a very large surface area and rich atomic steps, endowing the Au@Pt concave nanocube with good electrocatalytic properties.

CONCLUSION

In summary, we have developed a facile and effective method for fabricating concave Au@Pt nanocubes via a galvanic replacement process using preformed Au@Ag truncated nanocubes as templates. The as-prepared concave Au@Pt nanocubes exhibit a unique plasmonic optical property and catalytic activity higher than that of a commercial Pt black catalyst in the catalytic reduction of *p*-nitrophenol to *p*-aminophenol by $NaBH_4$, and most importantly, the as-prepared concave Au@Pt nanocubes exhibit significantly higher electrocatalytic activity and durability for the EOR in alkaline media than commercial Pt black. The as-synthesized concave Au@Pt nanocubes, because of their well-defined concave core−shell nanostructure and high-level electrocatalytic performance, will find promising potential applications in various fields, such as ethanol fuel cells.

ASSOCIATED CONTENT

Supporting Information

Histogram of the sizes of Au NPs, Au@Ag NPs, and concave Au@Pt NPs, HAADF-STEM image and the corresponding elemental mapping of Au@Ag and Au@Pt NPs, SAED pattern of the Au@Pt concave NPs, CVs of the Au NPs and Au@Ag electrodes in a 0.5 M H_2SO_4 solution, and comparisons of Au NPs, Au@Pt, and Pt black on the EOR. This material is available free of charge via the Internet at http://pubs.acs.org.

AUTHOR INFORMATION

Corresponding Author

*E-mail: ydjin@ciac.ac.cn.

Author Contributions

H.L. and H.W. contributed equally to this work. Experimental work was performed by H.L., H.W., Y.Z., and X.X. This work was directed and supervised by Y.J. This paper was written by H.L., H.W., and Y.J.

Notes

The authors declare no competing financial interest.

ACKNOWLEDGMENTS

Financial support by start-up funds from the Changchun Institute of Applied Chemistry, Chinese Academy of Sciences, the Hundred Talents Program of the Chinese Academy of Sciences, and the State Key Laboratory of Electroanalytical Chemistry (110000R387).

REFERENCES

(1) Gu, J.; Zhang, Y.-W.; Tao, F. *Chem. Soc. Rev.* **2012**, *41*, 8050−8065.
(2) Somorjai, G. A. *Chem. Rev.* **1996**, *96*, 1223−1236.
(3) Wu, H. X.; Wang, P.; He, H. L.; Jin, Y. D. *Nano Res.* **2012**, *5*, 135−144.
(4) Wu, H. X.; He, H. L.; Zhai, Y. J.; Li, H. J.; Lai, J. P.; Jin, Y. D. *Nanoscale* **2012**, *4*, 6974−6980.
(5) Liu, X. G.; Wang, D. S.; Li, Y. D. *Nano Today* **2012**, *7*, 448−466.
(6) Zhang, H.; Jin, M. S.; Xia, Y. N. *Chem. Soc. Rev.* **2012**, *41*, 8035−8049.
(7) Jin, Y. D.; Shen, Y.; Dong, S. J. *J. Phys. Chem. B* **2004**, *108*, 8142−8147.
(8) Zhang, G.-R.; Zhao, D.; Feng, Y.-Y.; Zhang, B. S.; Su, D. S.; Liu, G.; Xu, B.-Q. *ACS Nano* **2012**, *6*, 2226−2236.
(9) Peng, Z.; You, H.; Wu, J.; Yang, H. *Nano Lett.* **2010**, *10*, 1492−1496.
(10) Wu, J.; Zhang, J.; Peng, Z.; Yang, S.; Wagner, F. T.; Yang, H. *J. Am. Chem. Soc.* **2010**, *132*, 4984−4985.
(11) Yamauchi, Y.; Kuroda, K. *Chem.—Asian J.* **2008**, *3*, 664−676.
(12) Zhang, H.; Jin, M.; Xia, Y. *Chem. Soc. Rev.* **2012**, *41*, 8035−8049.
(13) Bigall, N. C.; Hartling, T.; Klose, M.; Simon, P.; Eng, L. M.; Eychmuller, A. *Nano Lett.* **2008**, *8*, 4588−4592.
(14) Wang, L.; Yamauchi, Y. *J. Am. Chem. Soc.* **2009**, *131*, 9152−9153.
(15) Yamauchi, Y.; Takai, A.; Nagaura, T.; Inoue, S.; Kuroda, K. *J. Am. Chem. Soc.* **2008**, *130*, 5426−5427.
(16) Takai, A.; Yamauchi, Y.; Kuroda, K. *J. Mater. Chem.* **2009**, *19*, 4205−4210.
(17) Song, Y. J.; Garcia, R. M.; Dorin, R. M.; Wang, H. R.; Qiu, Y.; Shelnutt, J. A. *Angew. Chem., Int. Ed.* **2006**, *45*, 8126−8130.
(18) Takai, A.; Yamauchi, Y.; Kuroda, K. *Chem. Commun.* **2008**, *44*, 4171−4173.
(19) Song, Y. J.; Steen, W. A.; Peña, D.; Jiang, Y. B.; Medforth, C. J.; Huo, Q. S.; Pincus, J. L.; Qiu, Y.; Sasaki, D. Y.; Miller, J. E.; Shelnutt, J. A. *Chem. Mater.* **2006**, *18*, 2335−2346.
(20) Yu, T.; Kim, D. Y.; Zhang, H.; Xia, Y. N. *Angew. Chem., Int. Ed.* **2011**, *50*, 2773−2777.
(21) Zhang, J.; Langille, M. R.; Personick, M. L.; Zhang, K.; Li, S. Y.; Mirkin, C. A. *J. Am. Chem. Soc.* **2010**, *132*, 14012−14014.
(22) Yu, Y.; Zhang, Q. B.; Lu, X. M.; Lee, J. Y. *J. Phys. Chem. C* **2010**, *114*, 11119−111126.
(23) Lu, C. L.; Prasad, K. S.; Wu, H. L.; Ho, J. A. A.; Huang, M. H. *J. Am. Chem. Soc.* **2010**, *132*, 14546−14553.
(24) Zhang, L.; Niu, W. X.; Li, Z. Y.; Xu, G. B. *Chem. Commun.* **2011**, *47*, 10353−10355.
(25) Niu, W. X.; Xu, G. B. *Nano Today* **2011**, *6*, 265−285.
(26) Zhang, L.; Niu, W. X.; Xu, G. B. *Nano Today* **2012**, *7*, 586−605.
(27) Wang, L.; Nemoto, Y.; Yamauchi, Y. *J. Am. Chem. Soc.* **2011**, *133*, 9674−9677.
(28) Lim, B.; Jiang, M.; Camargo, P. H. C.; Cho, E. C.; Tao, J.; Lu, X.; Zhu, Y.; Xia, Y. N. *Science* **2009**, *324*, 1302−1305.
(29) Peng, Z.; Yang, H. *J. Am. Chem. Soc.* **2009**, *131*, 7542−7543.
(30) Wu, H. X.; Li, H. J.; Zhai, Y. J.; Xu, X. L.; Jin, Y. D. *Adv. Mater.* **2012**, *24*, 1594−1597.
(31) Zhang, H.; Jin, M. S.; Wang, J. G.; Kim, M. J.; Yang, D.; Xie, Z. X.; Xia, Y. N. *J. Am. Chem. Soc.* **2011**, *133*, 10422−10425.

(32) Zhou, S. Z.; Mcllwrath, K.; Jackson, G.; Eichhorn, B. *J. Am. Chem. Soc.* **2006**, *128*, 1780−1781.
(33) Yamauchi, Y.; Tonegawa, A.; Komatsu, M.; Wang, H.; Wang, L.; Nemoto, Y.; Suzuki, N.; Kuroda, K. *J. Am. Chem. Soc.* **2012**, *134*, 5100−5109.
(34) Kim, Y.; Hong, J. W.; Lee, Y. W.; Kim, M.; Kim, D.; Yun, W. S.; Han, S. W. *Angew. Chem., Int. Ed.* **2010**, *49*, 10197−10201.
(35) Kristian, N.; Yan, Y. S.; Wang, X. *Chem. Commun.* **2008**, *44*, 353−355.
(36) Kristian, N.; Wang, X. *Electrochem. Commun.* **2008**, *10*, 12−15.
(37) Wang, S. Y.; Kristian, N.; Jiang, S. P.; Wang, X. *Nanotechnology* **2009**, *20*, 025605.
(38) Zhang, J.; Sasaki, K.; Sutter, E.; Adzic, R. R. *Science* **2007**, *315*, 220−222.
(39) Wang, L.; Yamauchi, Y. *J. Am. Chem. Soc.* **2010**, *132*, 13636−13638.
(40) Guo, S. J.; Sun, S. H. *J. Am. Chem. Soc.* **2012**, *134*, 2492−2495.
(41) Jin, Y. D.; Gao, X. H. *Nat. Nanotechnol.* **2009**, *4*, 571−576.
(42) Jin, Y. D.; Jia, C. X.; Huang, S. W.; O'Donnell, M.; Gao, X. H. *Nat. Commun.* **2010**, *1*, 41−48.
(43) Jin, Y. D.; Gao, X. H. *J. Am. Chem. Soc.* **2009**, *131*, 17774−17776.
(44) Yavuz, M. S.; Cheng, Y. Y.; Chen, J. Y.; Cobley, C. M.; Zhang, Q.; Rycenga, M.; Xie, J. W.; Kim, C.; Song, K. H.; Schwartz, A. G.; Wang, L. H. V.; Xia, Y. N. *Nat. Mater.* **2009**, *8*, 935−939.
(45) Schrinner, M.; Ballauff, M.; Talmon, Y.; Kauffmann, Y.; Thun, J.; Möller, M.; Breu, J. *Science* **2009**, *323*, 617−620.
(46) Ma, Y.; Li, W.; Cho, E. C.; Li, Z.; Yu, T.; Zeng, J.; Xie, Z.; Xia, Y. N. *ACS Nano* **2010**, *4*, 6725−6734.
(47) Sun, Y.; Mayers, B. T.; Xia, Y. N. *Nano Lett.* **2002**, *2*, 481−485.
(48) Sun, Y.; Mayers, B. T.; Xia, Y. *Adv. Mater.* **2003**, *15*, 641−646.
(49) Ataee-Esfahani, H.; Wang, L.; Nemoto, Y.; Yamauchi, Y. *Chem. Mater.* **2010**, *22*, 6310−6318.
(50) Ataee-Esfahani, H.; Nemoto, Y.; Wang, L.; Yamauchi, Y. *Chem. Commun.* **2011**, *47*, 3885−3887.
(51) Ataee-Esfahani, H.; Wang, L.; Yamauchi, Y. *Chem. Commun.* **2010**, *46*, 3684−3686.
(52) Feng, L. L.; Wu, X. C.; Ren, L. R.; Xiang, Y. J.; He, W. W.; Zhang, K.; Zhou, W. Y.; Xie, S. S. *Chem.—Eur. J.* **2008**, *14*, 9764−9771.
(53) Zhu, C. Z.; Guo, S. J.; Dong, S. J. *J. Mater. Chem.* **2012**, *22*, 14851−14855.
(54) Hu, C.; Cheng, H.; Zhao, Y.; Hu, Y.; Liu, Y.; Dai, L.; Qu, L. *Adv. Mater.* **2012**, *24*, 5493−5498.
(55) Qi, Z.; Geng, H.; Wang, X.; Zhao, C.; Ji, H.; Zhang, C.; Xu, J.; Zhang, Z. *J. Power Sources* **2011**, *196*, 5823.
(56) Zhang, G.-R.; Wu, J.; Xu, B.-Q. *J. Phys. Chem. C* **2012**, *116*, 20839−20847.
(57) Zhu, L. D.; Zhao, T. S.; Xu, J. B.; Liang, Z. X. *J. Power Sources* **2009**, *187*, 80−84.
(58) Han, X. Y.; Wang, D. W.; Liu, D.; Huang, J. S.; You, T. Y. *J. Colloid Interface Sci.* **2012**, *367*, 342−347.
(59) Li, M.; Liu, P.; Adzic, R. R. *J. Phys. Chem. Lett.* **2012**, *3*, 3480−3485.
(60) Ferrin, P.; Nilekar, A. U.; Greeley, J.; Mavrikakis, M.; Rossmeisl, J. *Surf. Sci.* **2008**, *602*, 3424−3431.
(61) Chen, L. Y.; Chen, N.; Hou, Y.; Wang, Z. C.; Lv, S. H.; Fujita, T.; Jiang, J. H.; Hirata, A.; Chen, M. W. *ACS Catal.* **2013**, *3*, 1220−1230.
(62) Wang, L.; Yamauchi, Y. *Chem.—Eur. J.* **2011**, *17*, 8810−8815.